Proceedings of the ASME 2015 International Mechanical Engineering Congress & Exposition
IMECE2015
November 13-19, 2015, Houston-TX

IMECE2015-51498

ENERGY CONVERSION ANALYSIS OF A NOVEL SOLAR THERMOCHEMICAL SYSTEM COUPLED WITH FUEL CELLS

Ian Vinck
KU Leuven, Mechanical Engineering Department
Leuven, 3001, Belgium

Nesrin Ozalp
KU Leuven, Mechanical Engineering Department
Leuven, 3001, Belgium

ABSTRACT

Fossil fuels have been the main supply of power generation for use in manufacturing, transportation, residential and commercial sectors. However, environmentally adverse effects of fossil fuel conversion systems combined with pending shortage raise major concerns. As a promising approach to tackle these challenges, this paper presents a novel energy conversion system comprising of a solar thermal reactor coupled with hydrogen fuel cell and carbon fuel cell for electricity generation. The system uses concentrated solar energy for high temperature heat which upgrades the calorific value of the feedstock by 8%. The paper describes the components and characteristics of the proposed concept and models the energy flow of this system. A comparison based on unit mass feedstock supply is made with conventional Brayton cycles for electricity production. The results show that the extent of acetylene by-product conversion in the solar reactor is of crucial importance to ensure competitiveness. Depending on the fuel cells efficiency and even more on the extent of byproduct formation, the results show that the overall chemical-to-electrical efficiency of this combined system ranges from 35 to 58%.

INTRODUCTION

Adverse environmental impacts of electricity production from fossil fuel combustion and consecutive increase in carbon taxation motivate the use of renewable energy sources for power generation. Traditionally, electricity is primarily produced by thermal power plants based on Rankine and Brayton cycles which are characterized by limited efficiencies. However, there are possible alternatives that offer better energy conversion efficiency and lower emissions, such as fuel cells. This paper presents a novel solar thermal system combined with hydrogen fuel cell and carbon fuel cell which performs more efficiently than traditional power generation systems.

Fuel cells convert chemical energy of fuel directly into electrical energy without intermediate thermal conversion steps. They are not limited by the Carnot efficiency which allows them to reach theoretical efficiencies of 100% per Gibbs-free energy and enthalpy of formation ratio. Practical chemical-to-electrical efficiencies of fuel cells range from 40% to more than 80% depending on fuel cell type and fuel [1]. Currently, hydrogen is the most common fuel for fuel cells. The overall reaction in a typical hydrogen fuel cell (H2FC) is given by Equation 1:

$$2\,H_2 + O_2 \rightarrow 2\,H_2O \qquad (1)$$

According to the electrolyte used and operating temperature, a wide range of different hydrogen fuel cell types exists such as Proton Exchange Membrane (PEMFC), Alkaline (AFC), Phosphoric Acid (PAFC), Molten Carbonate (MCFC) and Solid Oxide (SOFC) with efficiencies ranging from 40% to 65% as shown in Table 1.

Table 1 Overview of the current status of hydrogen FCs [2, 3]

Fuel cell	Operating temperature (°C)	Efficiency (%, LHV)	Capacity
PEMFC	60-180	40-60	1 W to 250 kW
AFC	0-230	50-70	10-100 kW
PAFC	200	40	100-200 kW, 1-2 MW
MCFC	650	50-65	100-250 kW, 1-2 MW
SOFC	800-1000	50-65	1-250 kW, 1.7 MW

As the table indicates; AFC, MCFC and SOFC are the most efficient hydrogen fuel cells with an average efficiency of 60%. Although the capacity of PAFC, MCFC and SOFC are in the megawatt range, only MCFC and SOFC are recommended for utility power plants [2]. Therefore, large stationary power

generation is generally done using MCFC [4]. Currently, PEMFCs have been receiving a lot of attention. They are well developed and already commercially available, whereas other fuel cell types are still in development stage. PEMFCs use a solid polymer as electrolyte in which protons (H+) are mobile and can only withstand temperatures up to 180°C [4].

Although hydrogen fuel cells still receive the most attention, direct carbon fuel cells (DCFC) are becoming increasingly attractive due their even better performance, reaching efficiencies up to 90%. In a DCFC, the solid carbon feed interacts electrochemically with oxygen gas, thereby forming carbon-dioxide gas as given by Equation 2:

$$C + O_2 \rightarrow CO_2 \quad (2)$$

As opposed to most other fuel cell types, DCFCs have distinct feed and product phases allowing the fuel utilization at almost 100%. DCFCs also take advantage of the fact that carbon has a very high volumetric energy density which is 19 kWh/L whereas it is 2.4 and 9.8 kWh/L for hydrogen and diesel fuel, respectively [4].

Another very important advantage of electricity generation via DCFCs is the fact that the product is pure CO_2 [1]. This offers considerable convenience because of eliminating carbon capture and storage (CCS). For example, fossil fuel-based power plants consume up to 30% of their electrical output for carbon sequestration [5].

In spite of their attractiveness, DCFCs experience three difficulties; *(1)* due to the solid phase fuel (carbon), *(2)* the reverse Boudouard reaction and 3) Impurity and ash content of the feedstock. Carbon complicates the necessary contact for electrochemical reactions to occur. Several methods have been developed to overcome this problem: *(1)* solid carbon rods serving simultaneously as fuel and anode, *(2)* fluidized carbon beds, *(3)* slurries by dispersing carbon in molten carbonates or molten metals [1], and *(4)* gasification of carbon by co-feeding a CO_2 stream [6].

As for the second issue, all DCFCs employ reverse Boudouard reaction as a side reaction:

$$C + CO_2 \rightarrow 2\,CO \quad (3)$$

This reaction is thermodynamically favored at temperatures above 705°C. It is of great importance in DCFCs as it is not an electrochemical reaction, thereby consuming carbon but not contributing to the cell potential. Moreover, because CO mixes with CO_2 it no longer gives pure outlet stream. However, Giddey et al. (2012) proposes several operating conditions to ensure fuel utilization ratio of 100%. For certain DCFCs, on the contrary, the reverse Boudouard reaction is desired because it gasifies carbon particles which enhance contact with the anode where the oxidation takes place.

For a given fuel cell type and temperature, the impurities and ash content of the carbon feed is extremely important for the performance and durability of DCFC [9]. This aspect currently hinders the use of biochar as a fuel in DCFCs [10]. Because the carbon produced by solar thermochemical decomposition of methane is very high purity, it possesses the best quality for use in DCFCs.

Based on the electrolyte used, there are three major groups of DCFCs: *(1)* molten salt (using KOH, NaOH), *(2)* molten carbonate (Li, Na, K) and *(3)* oxygen ion conducting ceramic (Solid Oxide). DCFCs are also characterized based on their working temperatures which are between 500 and 1000°C and fuel cell efficiencies ranging from 70 to 90% as seen in Table 2.

Table 2 An overview of DCFCs [1, 7, 8]

Fuel cell	**Operating temperature (°C)**	**Efficiency (%, LHV)**
Molten salt	500-600	70-90
Molten carbonate	750-800	
Oxygen ion conducting ceramic	500-1000	

Carbon production currently practiced in industry is basically based upon the “furnace” process which is not only highly energy intensive but also very polluting as seen in Table 3. Similarly, hydrogen production in industry requires large amounts of energy and emits toxic and greenhouse gasses into the environment during production process. Therefore, hydrogen and carbon feedstock for H2FCs and DCFCs should be produced solar thermochemically to reduce energy consumption and to eliminate hazardous emissions.

Table 3 An overview of hydrogen and carbon black production in industry [2, 11, 12, 13, 14]

Fuel	**Annual production (Million tons)**	**World market value (Billion $)**	**CO_2-eq emission (kg/kg production)**
Hydrogen	53 [12]	82.7 [2]	11.9 [11]
Carbon black	9 [13]	7-11 [14]	5.7 [11]

It is possible to produce hydrogen and carbon black with zero emissions footprint via direct solar thermal decomposition of methane which is being considered as the optimum route for sustainable production of these two valuable fuels [15]. This paper presents a novel system coupling hydrogen and carbon black producing solar thermal reactor with hydrogen and carbon fuel cells for sustainable, more efficient, and emission free generation of electricity.

HYDROGEN AND CARBON PRODUCTION VIA SOLAR THERMAL SPLITTING OF METHANE

The concept of co-producing hydrogen and carbon black by solar thermal decomposition of methane - also known as "solar cracking"- has been widely studied mainly by the research groups of Steinfeld of ETH-Zurich, Flamant of CNRS-PROMES, Weimer of Colorado, Kogan of Weizmann Institute of Science etc. [16-19]. Methane is the primary component of natural gas with approximately 95 mol % and is an excellent feedstock for hydrogen production to high hydrogen-to-carbon ratio.

The cracking reaction that decomposes methane into hydrogen and carbon is endothermic requiring 76 kJ heat per mole of decomposed methane when the reactants and reaction products are at temperature of 298 K [20].

$$CH_4 \rightarrow 2\,H_2 + C \quad (4)$$

Methane is a very stable molecule due to the strong C-H bonds (440 kJ/mol) and lack of polarity. Therefore, methane decomposition requires high temperatures in excess of 1200°C [21]. Thermodynamic studies done by Ref. [22] and Ref. [23] based on minimization of Gibbs-free energy show that decomposition of methane starts at 600 K and reaches to nearly complete conversion into hydrogen and carbon black at 1500 K. Trace-products include acetylene C_2H_2, ethylene C_2H_4, butylene C_4H_8, propylene C_3H_6, and ethane C_2H_6. However, kinetic studies based on the activation energy and transport processes show that higher temperatures are required in between 1500 K and 2000 K [24, 25-26]. Although there are several kinetic reaction mechanisms taking intermediates and by-product formation into account, the simplified reaction mechanism is a stepwise dehydrogenation as given in Equation 5 [20]:

$$2\,CH_4 \rightarrow C_2H_6 \rightarrow C_2H_4 \rightarrow C_2H_2 \rightarrow 2C \quad (5)$$

This explains the presence of acetylene which is up to 7% depending on residence time in incomplete conversion and has influence on carbon yield [27].

The advantages of solar cracking of methane over traditional hydrogen and carbon black production are the following:

(1) Since the reaction heat is provided by solar energy, no combustion of fossil fuels is required. Therefore, there is no discharge of pollutants.
(2) By the absorption of solar energy, the higher heating value of natural gas (ca. 890 kJ/mole) is in fact upgraded in an amount equal to the enthalpy change of the endothermic cracking reaction (75.6 kJ/mol) which yields an increase of 8%.
(3) Traditional steam reforming of methane requires 41.3 kJ of heat per mol hydrogen, whereas solar cracking of methane requires 37.8 kJ/mol H_2 which is a slight advantage. However, when the heat required for steam generation is taken into account, steam reforming of methane requires 63 kJ/mol H_2 which is significantly higher.
(4) The resulting product hydrogen (gas) and (solid) carbon are distinct phases, making them easily separable and preventing hydrogen contamination.
(5) Solar cracking of methane yields carbon which is a very valuable product making H_2 production more competitive.

As for carbon black, it is a very pure form of carbon characterized by a disordered structure. Carbon black is very valuable not only as commodity but also as fuel for DCFCs. As tested by Ref. [28], it contains around 98 wt% carbon and less than 0.001 wt% ashes. This presents very big advantage for use in DCFCs because impurities tend to lower DCFCs performance drastically. Also, Ref. [29] and Ref. [28] show that a disordered structure as seen in Figure 1 improves the reactivity as a result of higher concentration of defects and edge atoms.

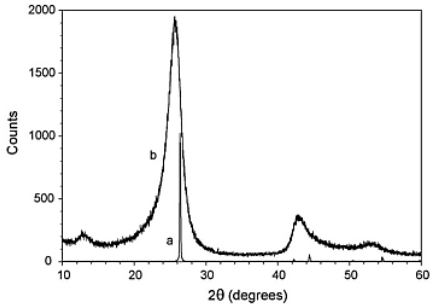

(a)

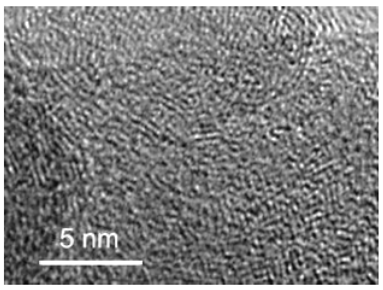

(b)

Figure 1: (a) XRD of graphite "a" and carbon black produced by thermocatalytic decomposition of methane "b". **(b)** TEM image of carbon black produced by thermocatalytic decomposition of methane. Both figures are obtained from Ref. [29].

Another advantage of carbon black is its very large surface area which is 31.34 m^2/g. Compared to the surface area of graphite which is 0.21 m^2/g, and coal types which are about 6.65 m^2/g; carbon black exhibits higher potential for reactivity [28]. This makes carbon black the ideal fuel for DCFCs. It is shown by Ref. [27] that the carbon produced by solar cracking

of methane is comparable to commercially available carbon black quality.

DESCRIPTION OF THE SOLAR REACTOR SYSTEM COUPLED WITH FUEL CELLS

The main components of the proposed system are illustrated in Figure 2. The system is mainly consists of a Concentrating Solar Power (CSP) unit to focus the sunlight onto the reactor window, a scrubber eliminating sulfurous compounds present in natural gas feed, a solar reactor in which the solar cracking reaction given in Equation 4 takes place, a baghouse filter which separates the solid carbon from the gaseous products and a Pressure Swing Adsorption (PSA) device which purifies the hydrogen gas (up to 99.999 mol %) before it enters the hydrogen fuel cell. For simplicity the compressors and heat exchangers to preheat the natural gas feed and cool down the products are omitted in the figure. This system basically uses natural gas as the main feedstock where it is solar thermally decomposed into hydrogen and carbon black with zero emission. As aforementioned, solid carbon black and hydrogen gas are easily separated for use in fuel cells.

The concentrating solar energy facility in this system could be a tower or a dish. Their capability of concentrating solar energy Q_{solar} over an area A and normalized w.r.t. the incident normal beam insolation I is expressed by the solar concentration ratio C given by the following equation

$$C = \frac{Q_{solar}}{IA} \tag{6}$$

When normalized to 1 kW/m^2, C is often expressed in units of "suns", e.g. 1 kW/m^2. For tower systems, typical concentration values range in between 500 and 5,000 suns whereas it ranges between 1,000 and 10,000 suns for dish systems. This can be augmented to some extent by using secondary concentrators. Because trough systems are only capable of achieving 400–550°C, they cannot be used for solar cracking of methane [15]. As for the solar reactor of the proposed system, a directly heated reactor concept can be used as illustrated in Figure 3.

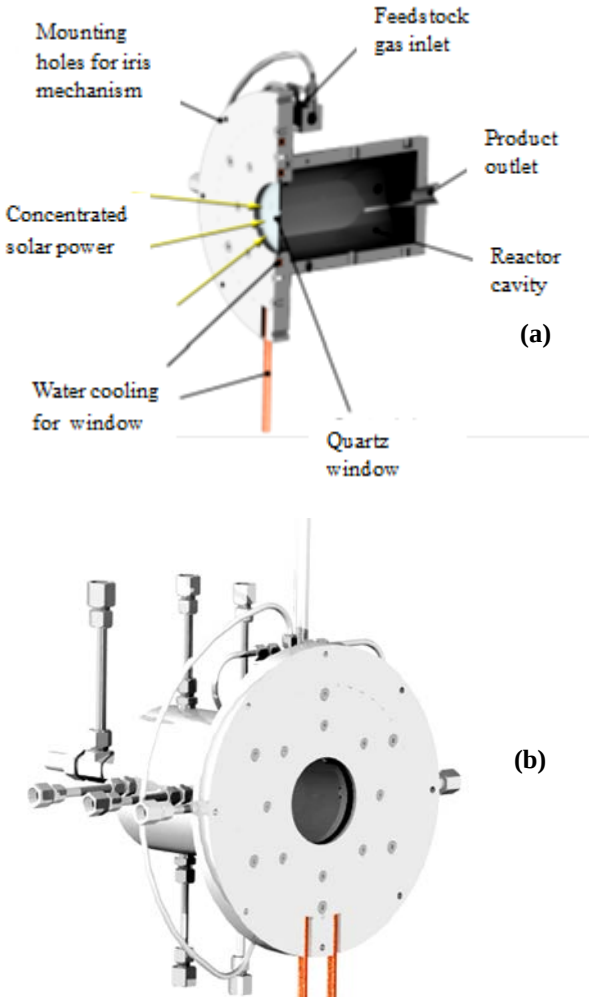

Figure 3: An example directly heated solar reactor designed at Solar Thermal Technology Laboratory (STTL) of KU Leuven. **(a)** Cross sectional view, **(b)** Assembled view.

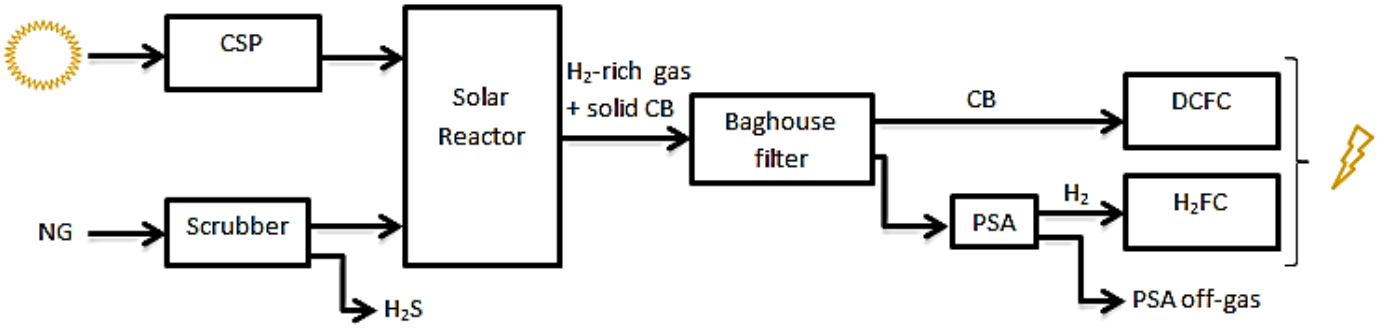

Figure 2: Illustration of the hybrid energy conversion system driven by solar reactor produced hydrogen and carbon black as feedstocks of fuel cells

COMPONENT BASED MODELING OF THE SYSTEM

The model used in this analysis is shown in Figure 4. Scrubber unit for cleaning the natural gas inlet to the reactor is neglected due to its small impact on energy and flow rates. The resulting model thus consists of the following components:

- *Solar reactor:* housing solar thermal decomposition reaction.
- *Baghouse filter:* separation of carbon black particles from gaseous products.
- *PSA:* Pressure Swing Adsorption for separation of hydrogen from other product gasses.
- *DCFC:* Direct Carbon Fuel Cell fed with carbon black produced by the solar reactor.
- *H2FC:* Hydrogen Fuel Cell.
- *Vacuum compr:* ensures subatmospheric reactor pressure
- *HEx 1:* Heat exchanger 1 for cooling products coming out of the solar reactor to the operating temperature of the baghouse filter, by water and argon (for preheating carbon in HEx2)
- *HEx 2 and Mixer 1:* HEx2 preheats the carbon particles. In Mixer 1, they are mixed with hot recycled CO_2 from the DCFC anode exhaust, for further heating and transportation.
- *HEx 3:* Air heating unit.
- *HEx 4, 7 and Compr 2, 3:* heating and compression of the hydrogen gas and humidified air to operating temperature of the hydrogen fuel cell.
- *HEx 5,6 and Compr 1a, 1b:* two-stage compression with intercooling prior to PSA.
- *Humidifier:* assures the correct humidity for the H2FC.

In the model, all pressure drops and heat losses in between components are neglected. Temperature and pressure of the outlet of the forgoing component are assumed to be equal to the inlet temperature and pressure of the next component.

Solar reactor: In order to ensure reliable results, experimental data from Ref. [30] and Ref. [17] are taken which is based on experiments using a 50 kW tubular solar reactor tested at 1 MW solar furnace of CNRS-PROMES. The reactor is an indirect heating type of graphitic tubular geometry tested in temperature range of 1608 K to 1928 K, and residence times of 37 to 71 ms. The solar power input intercepted by the reactor is in between 23 kW and 37 kW. As a result of Le Chatelier's principle, the reactor is operated at sub-atmospheric pressures, e.g. between 41 kPa and 47 kPa. Each of the seven reactor tubes is fed with a mixture of methane and argon. Table 4 summarizes the feed and operating conditions of the reactor for all nine experimental runs executed and Table 5 gives the off-gas composition and chemical performance obtained by Ref. [30].

Table 4 Experimental configuration used in analysis from [30]

	Ar (Nl/min)	CH_4 (Nl/min)	CH_4 mol frac.	Pres. (kPa)	Temp. (K)	Resid. time (s)
Run 1	31.5	10.5	0.25	43,000	1,608	0.07
Run 2	31.5	10.5	0.25	46,000	1,693	0.071
Run 3	31.5	10.5	0.25	43,000	1,778	0.063
Run 4	31.5	10.5	0.25	42,000	1,793	0.061
Run 5	31.5	10.5	0.25	42,000	1,928	0.057
Run 6	49	21	0.3	47,000	1,698	0.043
Run 7	21	21	0.5	41,000	1,798	0.059
Run 8	49	21	0.3	43,000	1,808	0.037
Run 9	49	21	0.3	45,000	1,873	0.038

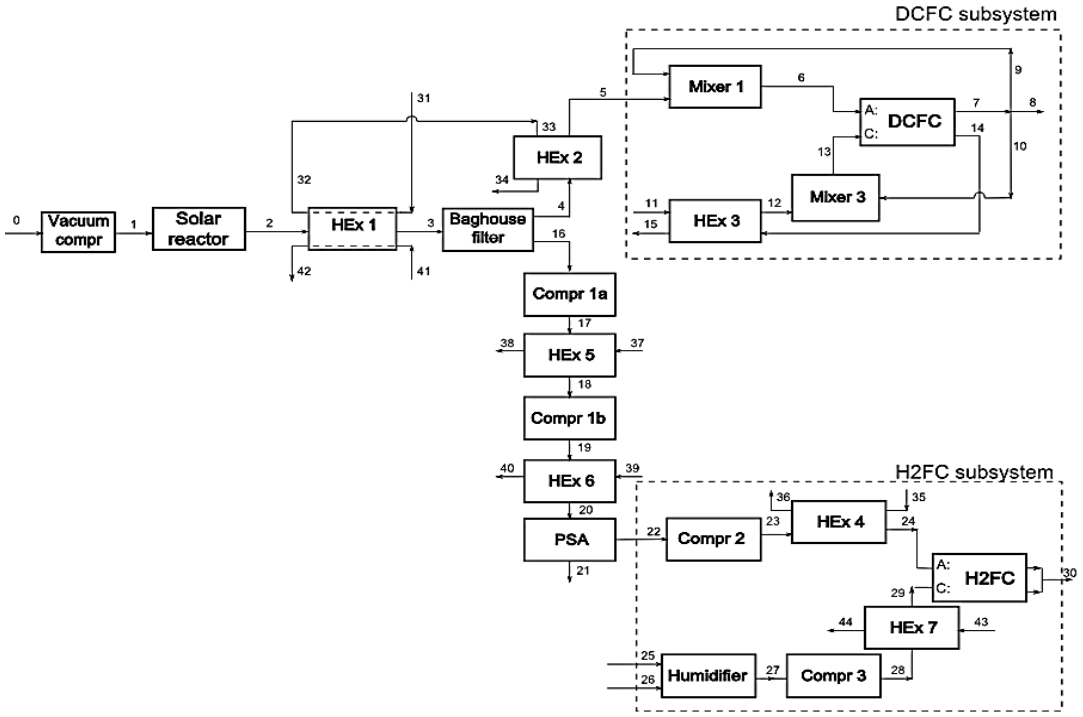

Figure 4: Schematic of the model with labels of both fuel cell subsystems (HEx : Heat exchanger, Compr. : compressor, PSA : Pressure Swing Adsorption unit, A: anode, C: cathode)

Table 5 Experimental data from Ref. [30].

	Off-gas compositions (mol fractions)					Chemical performance		
	H_2	CH_4	C_2H_4	C_2H_6	C_2H_2	X_{CH4}	Y_{H2}	Y_C
Run 1	0.25	0.06	0.0022	0.0002	0.0291	0.72	0.57	0.43
Run 2	0.32	0.01	0.0029	0.0001	0.0432	0.95	0.77	0.5
Run 3	0.33	0	0.0026	0	0.0478	0.99	0.79	0.5
Run 4	0.32	0	0.0023	0.0001	0.0496	0.99	0.81	0.47
Run 5	0.34	0	0.0019	0	0.0363	1	0.81	0.63
Run 6	0.31	0.06	0.0029	0.0005	0.0394	0.75	0.62	0.41
Run 7	0.55	0.01	0.0036	0.0002	0.0727	0.98	0.88	0.49
Run 8	0.37	0.02	0.0023	0	0.0588	0.94	0.77	0.42
Run 9	0.38	0.01	0.002	0.0001	0.0598	0.97	0.79	0.45

It is important to note that a methane feed is used instead of natural gas and that argon is co-fed. However, Ref. [31] reports that there is no difference between using methane or natural gas as feedstock for residence times longer than 1 ms. Below 1 ms, a small difference is expected due to the presence of ethane in natural gas (about 9.5% ethane and trace amounts of CO_2 and N_2), which decomposes easier than methane.

Argon is co-fed in substantial mol fractions between 50% and 75% in order to prevent carbon deposition on reactor tubes. Although argon is an inert gas and it does not interact chemically, it influences the heat balance inside the reactor by absorbing heat.

In order to evaluate the reactor performance as well as to know the amounts of all products formed, following concepts are used in present work to calculate methane conversion, hydrogen yield and carbon yield as defined by Equations 7 to 9 respectively.

$$X_{CH_4} = \frac{\dot{N}_{0,CH_4} - \dot{N}.y_{CH_4}}{\dot{N}_{0,CH_4}} \tag{7}$$

$$Y_{H_2} = \frac{\dot{N}.y_{H_2}}{2.\dot{N}_{0,CH_4}} \tag{8}$$

$$Y_C = \frac{\dot{N}_{0,CH_4} - (\dot{N}.y_{CH_4} + 2.\dot{N}.y_{C_2H_2} + 2.\dot{N}.y_{C_2H_4} + 2.\dot{N}.y_{C_2H_6})}{\dot{N}_{0,CH_4}} \tag{9}$$

where $\dot{N}$ is the molar flow rate of the outlet, $\dot{N}_0$ is the molar inlet flow rate, and y_i is the molar fraction of component *i*.

Direct Carbon Fuel Cell: Although several DCFC types are available, practically validated data is still absent. There are few theoretical models found in literature providing necessary inlet and outlet conditions for thermodynamic analysis such as Ref. [32] and Ref. [33]. However, there is critical need for more extensive and profound research in this domain in order to obtain experimental data that can be used in calculations to serve as reference.

Figure 4 shows the DCFC subsystem of the proposed hybrid system. The model for this subsystem is based on the following assumptions:

- DCFC is molten carbonate type
- Operating temperature is 750°C
- There is temperature rise of 100°C from the inlet to outlet due to exothermicity of the electrochemical reactions, e.g. T_{in} = 700°C, and T_{out} = 800°C.
- Steady state (initial heating up to reach operating temperature is not considered).
- Feeding rate of 1 kg/s pure carbon.
- Anode inlet stream is a mixture of CO_2 with 0.84 wt% carbon particles dispersed.
- Cathode inlet stream is a mixture of CO_2 and air, containing 0.19 wt% CO_2.
- 49.7 kg/s of air is required per kg/s carbon fed.
- Anode outlet is pure CO_2.
- Cathode outlet contains 4 mol % CO_2.
- Fuel utilization ratio FUR = 1.
- Cell voltage V_c = 0.8 V.

Based on these assumptions, all flow rates and temperatures are known. It is important to note that both anode and cathode inlets contain CO_2. At the cathode, this is in order to allow the formation of carbonate ions which are essential to the electrochemical reaction. At the anode, CO_2 is co-fed to transport carbon and enhance contact and therefore the reaction with the anode. This CO_2 co-feed is obtained by recycling hot anode exhaust. It is also important to note that the composition of air changes throughout the fuel cell. This is because oxygen is partly consumed and most of the CO_2 fed to the cathode travels through the electrolyte as carbonate ions, and leaves the anode as CO_2.

Hydrogen Fuel Cell: Although MCFCs are mostly used for stationary power applications, they are not fully developed yet. Therefore, there is lack of practical data as literature survey and mail correspondence with several prominent scientists in the field confirmed. Similar to the DCFCs field, there is crucial need for more profound research in the domain of MCFCs and other fuel cell types. In order to base the analysis on reliable and practical information, present work takes PEMFC which are commercially available. However, PEMFCs have lower efficiencies than MCFCs and therefore, as far as the H2FC is considered, the combined system efficiency will be lower than that of comprising MCFCs.

Baghouse filter: The outlet of the solar reactor is composed of a mixture of gasses which are primarily made of hydrogen, unconverted methane, and acetylene and solid carbon particles carried by the flow. The baghouse filter separates the carbon particles from the gasses. Depending on the specific filter type

and source, the maximal operating temperature is between 40°C and 180°C. Ref. [11] suggests an operating temperature of 50°C. Another aspect is the pressure drop over the filter. Ref. [11] suggests a pressure drop of 20 kPa. However, in present work, the pressure drop is neglected.

PSA: Since hydrogen fuel cells generally work only on pure hydrogen (and on methane if internal reforming is possible), all gasses other than hydrogen need to be removed from the reactor outlet, i.e., C_2H_2, C_2H_4 and C_2H_6 and unconverted methane. A Pressure Swing Adsorption unit (PSA) allows purification of hydrogen up to 99.999 mol % per stage [11] based on different adsorption characteristics of gasses under high pressure. After pressure builds up, effective separation is achieved by gradually reducing the pressure while each gas is released at different pressure. In general, PSA devices operate at near-ambient temperatures which remain almost constant throughout the device and pressure changes between 10 bars to 40 bars [34]. This high pressure is clearly disadvantageous in terms of energy requirement (compressor power), but is inherent to the separation process.

MODEL CALCULATIONS AND ENERGY ANALYSIS

Aforementioned model calculations are done by assuming that all pressure drops and heat losses between the components are negligible. The efficiency of the combined system presented in this paper is defined as the ratio of the electrical power output of both fuel cells and the chemical power input to the solar reactor via the methane feed as follows:

$$\eta = \frac{P_{PEMFC} + P_{DCFC} - P_{loss}}{P_{CH_4}} \tag{10}$$

where P_{loss} refers to the compressor power.

Compressor losses are calculated from:

$$P_{loss} = \dot{m}\, c_p \frac{T_1}{\eta_c}\left[\left(\frac{P_2}{P_1}\right)^{\frac{\gamma-1}{1}} - 1\right] \tag{11}$$

where $\dot{m}$ is the mass flow rate, c_p is the heat capacity at constant pressure, T_1 is the temperature before compression, P_1 and P_2 are the pressures before and after the compression, and γ is the ratio of specific heats. In order to calculate the power outputs of both fuel cells, the mass flow rates of their fuel inputs are calculated. Based on the methane conversions, hydrogen and carbon yields as well as the methane feeding rate given by Tables 4 and 5, all mass flow rates out of the reactor are known as compiled in Table 6.

Power outputs fuel cells: Apart from the mass flow rates in Table 6 and the lower heating values of carbon black and hydrogen, the power output of the fuel cells depends on the efficiency of the specific fuel cell type. For both fuel cells, power outputs are calculated over efficiency span, i.e. between 70% and 90% for DCFC, and, between 40% and 60% for PEMFC. Referring to Ref. [32], approximately 80% is taken as a reference DCFC efficiency). For the PEMFC, an open cell voltage of V_c = 0.65 V and fuel utilization coefficient of μ_f = 0.85 are assumed, yielding a reference PEMFC efficiency of approximately 45, according to Ref. [35]. This is rounded to 45% as reference PEMFC efficiency. In addition, power outputs are calculated assuming that all acetylene byproduct is fully converted to carbon black and hydrogen. Tables 7 and 8 give the power outputs calculated for each fuel cell.

Efficiency of the combined system: The chemical-to-electrical efficiency of the combined system is calculated by using the lower heating value of methane and Equation 10. Acetylene conversions in different cases are also taken into consideration. The results for different runs and cases are shown in Table 9.

Table 6 The total, hydrogen, carbon black and acetylene molar flow rates $\dot{N}$ (mol/s) and mass flow rates $\dot{M}$ (kg/s). The last row gives the mass flow rate of carbon black assuming full acetylene conversion.

Run	**1**	**2**	**3**	**4**	**5**	**6**	**7**	**8**	**9**
$\dot{N}_{tot,\,out}$	3.6×10^{-2}	3.8×10^{-2}	3.7×10^{-2}	4.0×10^{-2}	3.7×10^{-2}	6.3×10^{-2}	5.0×10^{-2}	6.5×10^{-2}	6.5×10^{-2}
$\dot{N}_{H2}$	8.9×10^{-3}	1.2×10^{-2}	1.2×10^{-2}	1.3×10^{-2}	1.3×10^{-2}	1.9×10^{-2}	2.8×10^{-2}	2.4×10^{-2}	2.5×10^{-2}
$\dot{N}_{CB}$	3.4×10^{-3}	3.9×10^{-3}	3.9×10^{-3}	3.7×10^{-3}	4.9×10^{-3}	6.4×10^{-3}	7.7×10^{-3}	6.6×10^{-3}	7.0×10^{-3}
$\dot{N}_{C2H2}$	2.1×10^{-3}	3.3×10^{-3}	3.6×10^{-3}	3.9×10^{-3}	2.7×10^{-3}	4.9×10^{-3}	7.3×10^{-3}	7.7×10^{-3}	7.8×10^{-3}
$\dot{M}_{H2}$	1.8×10^{-5}	2.0×10^{-5}	2.5×10^{-5}	2.6×10^{-5}	2.6×10^{-5}	3.9×10^{-5}	5.6×10^{-5}	4.9×10^{-5}	5.0×10^{-5}
$\dot{M}_{CB}$	4.0×10^{-5}	4.7×10^{-5}	4.7×10^{-5}	4.4×10^{-5}	5.9×10^{-5}	7.7×10^{-5}	9.2×10^{-5}	7.9×10^{-5}	8.5×10^{-5}
$\dot{M}_{CB,\,fc}$	6.5×10^{-5}	8.6×10^{-5}	9.0×10^{-5}	9.1×10^{-5}	9.2×10^{-5}	1.4×10^{-4}	1.8×10^{-4}	1.7×10^{-4}	1.8×10^{-4}

Table 7 DCFC power output (in *W*) for several all 9 experimental runs
(first row is the chemical input power based on the LHV of carbon, the subscript 'f_c' refers to full acetylene conversion)

Run	**1**	**2**	**3**	**4**	**5**	**6**	**7**	**8**	**9**
P_{in}	1,324	1,539	1,539	1,447	1,939	2,524	3,017	2,586	2,770
$P_{70\%}$	927	1,077	1,077	1,013	1,357	1,767	2,112	1,810	1,939
$P_{80\%}$	1,059	1,231	1,231	1,157	1,551	2,019	2,413	2,069	2,216
$P_{90\%}$	1,191	1,385	1,385	1,302	1,745	2,272	2,715	2,327	2,493
$P_{80\%,fc}$	1,712	2,255	2,358	2,394	2,403	3,572	4,705	4,482	4,657

Table 8 H2FC power output (in *W*) for several all 9 experimental runs
(first row is the chemical input power based on the LHV of hydrogen, the subscript 'f_c' refers to full acetylene conversion)

Run	**1**	**2**	**3**	**4**	**5**	**6**	**7**	**8**	**9**
P_{in}	2,157	2,913	2,989	3,065	3,065	4,692	6,659	5,827	5,978
$P_{40\%}$	863	1,165	1,196	1,226	1,226	1,877	2,664	2,331	2,391
$P_{45\%}$	953	1288	1321	1355	1355	2074	2943	2575	2642
$P_{50\%}$	1,078	1,457	1,494	1,532	1,532	2,346	3,329	2,913	2,989
$P_{60\%}$	1,294	1,748	1,793	1,839	1,839	2,815	3,995	3,496	3,587
$P_{45\%,\,fc}$	1,083	1,488	1,540	1,593	1,526	2,380	3,393	3,039	3,112

Table 9** Combined system efficiencies for all runs and different cases.
'Avg.' denotes the average of 1 case over all runs, 'Avg.*' is the average over all runs except 1 and 6.
Subscript 'f_c' indicates that full acetylene conversion is assumed.

Run	**1**	**2**	**3**	**4**	**5**	**6**	**7**	**8**	**9**	**Avg.**	**Avg.***
$\eta_{45,80}$	24	31	31	31	37	25	36	29	31	30	32
$\eta_{40,80}$	22	29	29	28	35	23	33	26	28	28	30
$\eta_{50,80}$	25	33	34	33	39	27	38	31	32	32	34
$\eta_{60,80}$	28	37	38	37	44	30	43	35	37	37	39
$\eta_{45,70}$	21	28	29	28	34	23	34	27	28	28	30
$\eta_{45,90}$	26	33	34	33	40	27	38	31	32	33	34
$\eta_{45,80,fc}$	36	50	52	53	53	39	57	51	53	49	53

** Different cases are indicated by $\eta_{x,\,y}$ where x denotes the PEMFC efficiency and y the DCFC efficiency.

Theoretical optimum efficiency: In order to make a comparison with what is maximally achievable in theory, Table 10 gives optimal efficiencies obtained when methane would react exactly corresponding to Equation 7, yielding 0.25 kg H_2 and 0.75 kg carbon black per kg methane. Three cases are being considered:

(1) 'Lower limit' using the poorest fuel cell efficiencies, e.g. 40 % for PEMFC and 70% for DCFC.

(2) 'Higher limit' using best fuel cell performances, e.g. 60% for PEMFC and 90% for DCFC.

(3) 'Practical case' where PEMFC efficiency is 45% and DCFC efficiency is 80%.

Table 10 Theoretical optimal efficiencies for three cases

Case	'Lower limit'	'Practical case'	'Higher limit'
$\eta_{optimum}$ *(%)*	51	59	72

RESULTS AND DISCUSSIONS

Combined system efficiency: Results for combined system efficiency are given in Tables 9–12. When compressor losses are taken into account, the combined system efficiency ranges from 24% to 37% for reference case where PEMFC has 45% efficiency and DCFC has 80% efficiency. If same amount of methane is used in conventional power generation cycles, a gas turbine cycle yields 26% efficiency whereas a combined cycle yields 56% efficiency (Ref. [36]). This shows that the proposed system comprising a solar reactor coupled with fuel cells performs better than gas turbine cycles whereas combined cycle exhibit higher performance.

The reason for getting relatively lower efficiency than a combined cycle is because of incomplete methane conversions in experiments. Referring to the results by the Flamant group of CNRS where the experimental data is taken from, it is seen that methane is not always converted fully and a significant part is converted into compounds other than carbon black and hydrogen. For example, methane conversion efficiency of Run 1 is 72% whereas Run 6 has 75% methane dissociation. The reason for low conversion efficiencies is because of high flow rate of argon cooling the reactor temperature and decreasing the residence time. Due to these suboptimal conditions, runs 1 and 6 are not considered in the analysis. Apart from Run 1 and Run 6, all other runs have conversion efficiencies between 98% and 100%.

The main factor affecting combined system efficiency is the formation of byproducts, primarily C_2H_2 and secondarily C_2H_4 and C_2H_6. Table 5 gives the mol fractions of these byproducts which are calculated by including argon presence. Methane feed is diluted by 50% to 75 mol% argon. Once this dilution is taken into account, mole fractions are between 8.5 % and 13.5 mol% as seen in Table 11. This is a considerable fraction because every mole of C_2H_2 prevents formation of 2 moles of carbon black and 1 mole of hydrogen. In practice, nearly full C_2H_2 dissociation can be achieved by prolonging the residence time.

Table 11 Acetylene and hydrogen mole fractions when there is zero Argon dilution.
('Avg' refers to the average of all 9 runs)

Run	y_{C2H2} (mol%, no Argon)	y_{H2} (mol%, no Argon)
1	8.47	72.79
2	11.43	84.67
3	12.76	88.07
4	12.14	78.31
5	9.77	91.48
6	9.43	74.18
7	10.56	79.92
8	13.36	83.98
9	13.55	86.37
Avg	11.27	82.20

If 100% acetylene dissociation is assumed, then the electricity production by DCFC increases. Neglecting Run 1 and Run 6 for the aforementioned, efficiencies between 50% and 57% can be obtained. Therefore, combined system outperforms traditional power cycles if all acetylene is dissociated.

Sensitivity analysis: Sensitivity analysis of the parameters involved allows determining the crucial factor in system efficiency. A system comprising 45% efficiency PEMFC and 80% efficiency DCFC is taken as the reference case for the sensitivity analysis. Parameters involve fuel cell efficiencies as well as acetylene conversion. By changing one parameter at a time, change in system efficiency is tabulated shown in Table 12.

Table 12 Sensitivity analysis of combined system efficiency with fuel cell efficiencies and acetylene conversion (subscript f_c refers to full acetylene conversion, Avg. refers to average the average over all runs except 1 and 6, and $\Delta\eta$ refers to efficiency change).

$\eta_{PEMFCeff.\ DCFCeff.}$	Avg. (%)	Parameter change	$\Delta\eta$ (%)
$\eta_{45,\ 80}$	32.1	reference	reference
$\eta_{40,\ 80}$	29.8	PEM: –5%	–7.5
$\eta_{50,\ 80}$	34.3	PEM: +5%	+6.6
$\eta_{60,\ 80}$	38.8	PEM: +10%	+17.4
$\eta_{45,\ 70}$	29.6	DC: –10%	–8.2
$\eta_{45,\ 90}$	34.5	DC: +10%	+7.0
$\eta_{45,\ 80,fc}$	52.7	Full C_2H_2 conv.	+39.2

It is clear from Table 12 that acetylene conversion has a major influence on combined system efficiency. Compared to the reference case, full acetylene conversion yields 39% increase in system efficiency. Although PEMFC and DCFC efficiencies are important, their impact on the overall system efficiency is much smaller. Therefore, the reactor conversion is the most critical component of this hybrid system.

An alternative operation mode of this hybrid system can provide continuous function including night time. For example, carbon black produced during the day time can be used during the night time to fuel DCFC. Electricity produced by the DCFC during the night time can be used to supply high temperature process heat for the reactor to continue methane decomposition during the times when solar energy is not available. In theory, approximately 0.05 kg/s carbon black (or 4.17 mol/s) is required for DCFC to deliver enough electricity to supply high temperature process heat needed to continuously produce 1 mol hydrogen per second. Subtracting the carbon black produced overnight, 0.04 kg carbon black per second from the night time operation would be sufficient to run the system over the night. If a power plant can provide this amount during day time, 24 hour operation is guaranteed.

CONCLUSIONS

A novel hybrid energy conversion system comprising a solar reactor, hydrogen fuel cell and carbon fuel cell was presented. State of the art in fuel cells, traditional electricity generation, and hydrogen and carbon black production were given. The system components were described, a model was constructed and an efficiency analysis was performed based on experimental reactor data in order to assess competitiveness of this system for electricity production. It was noted that there is crucial need for more extensive research in various hydrogen fuel cell and carbon fuel cell types.

An overview of the proposed system components was presented and chemical-to-electrical efficiency of the combined system was determined based on experimental data from literature. Solar reactor was identified as the most crucial system component to achieve high performance. Specifically, it was found that conversion of acetylene has a major influence on system efficiency. It was calculated that an efficiency increase of 39% can be obtained if acetylene is fully converted. Such case enable the proposed system outperform traditional power generation cycles. Therefore, it was concluded that methane cracking reactor must be researched in detail and developed to achieve full conversion of acetylene.

It was also noted that the system has the potential for operation on 24/7 basis when carbon black produced during the day time is being used in night time to run the DCFC for electrically provided high temperature process heat requirement of the reactor. As for the pure CO_2 output of the DCFC, it is possible to implement dry reforming of natural gas by using extra natural gas to combine with CO_2, which produces syngas.

Another important alternative use of this proposed system is the revenue from the unused carbon black. Because the carbon black production from methane cracking yields 75% of the products by mass, excess production of carbon black can be sold into market to leverage the operation costs of this system.

In conclusion, the solar thermal decomposition of natural gas for simultaneous production of hydrogen and carbon saves 277 MJ of fossil fuels per kg H_2 and results in an emission reduction of 13.9 kg of CO_2 per kg H_2 [11] compared to the traditional methods of hydrogen and carbon black production in industry. By coupling fuel cells to solar methane cracking reactor, this paper shows that overall electricity generation efficiency in the range of 50% to 57% can be obtained which is competitive with the current combined cycles.

REFERENCES

[1] S. Giddey, S.P.S. Badwal, A. Kulkarni, and C. Munnings, “A comprehensive review of direct carbon fuel cell technology,” Prog. Energy Combust. Sci., vol. 38, no. 3, pp. 360–399, Jun. 2012.

[2] A. Kirubakaran, S. Jain, and R.K. Nema, “A review on fuel cell technologies and power electronic interface,” Renew. Sustain. Energy Rev., vol. 13, no. 9, pp. 2430–2440, Dec. 2009.

[3] J.M. Beér, “High efficiency electric power generation: The environmental role,” Prog. Energy Combust. Sci., vol. 33, no. 2, pp. 107–134, Apr. 2007.

[4] J. Larminie and A. Dicks, Fuel Cell Systems Explained. West Sussex, England: John Wiley & Sons, Ltd., 2003.

[5] A. Steinfeld and A. Meier, “Solar fuels and materials,” Encycl. Energy, vol. 5, pp. 623–637, 2004.

[6] E.P. Agency, C. Protection, P. Division, and E.N. Group, “Technology Characterization : Steam Turbines,” no. March, 2002.

[7] W. Yan and S.K. Hoekman, “Production of CO_2 free hydrogen from methane dissociation : A review,” vol. 33, no. 1, 2014.

[8] O.Z. Sharaf and M.F. Orhan, “An overview of fuel cell technology: Fundamentals and applications,” Renew. Sustain. Energy Rev., vol. 32, pp. 810–853, Apr. 2014.

[9] A.C. Rady, S. Giddey, S.P. S. Badwal, B. P. Ladewig, and S. Bhattacharya, “Review of Fuels for Direct Carbon Fuel Cells,” Energy & Fuels, vol. 26, no. 3, pp. 1471–1488, Mar. 2012.

[10] C.E. Brewer, K. Schmidt-Rohr, J.A. Satrio, and R.C. Brown, “Characterization of Biochar from Fast Pyrolysis and Gasification Systems,” Environ. Prog. Sustain. Energy, vol. 28, no. 3, pp. 404–409, 2009.

[11] J. Wyss, J. Martinek, and M. Kerins, “Rapid Solar-thermal Decarbonization of Methane in a Fluid-wall Aerosol Flow

Reactor-Fundamentals and Application," Chem. React., vol. 5, no. A69, 2007.
[12] "Global Hydrogen Generation Market worth $118 Billion by 2016," Retrieved from: www.asdreports.com/news.asp?pr_id=874.
[13] P. Smithers, "The future of carbon black to 2015: global market forecasts," Retrieved from: www.smitherspira.com.
[14] R. Adams, "World carbon black demand forecast to go on notching up 4% annual growth," Focus Pigment., vol. 2006, no. 6, 2006.
[15] N. Ozalp, A. Kogan, and M. Epstein, "Solar decomposition of fossil fuels as an option for sustainability," Int. J Hyd. En., vol. 34, no. 2, pp. 710–720, 2009.
[16] G. Maag, G. Zanganeh, and A. Steinfeld, "Solar thermal cracking of methane in a particle-flow reactor for the co-production of hydrogen and carbon," Int. J Hyd. En., vol. 34, no. 18, pp. 7676–7685, 2009.
[17] S. Rodat, S. Abanades, E. Grivei, G. Patrianakos, A. Zygogianni, A.G. Konstandopoulos, and G. Flamant, "Characterisation of carbon blacks produced by solar thermal dissociation of methane," Carbon, vol. 49, no. 9, pp. 3084–3091, 2011.
[18] J.K. Dahl, K.J. Buechler, A.W. Weimer, A. Lewandowski, and C. Bingham, "Solar-thermal dissociation of methane in a fluid-wall aerosol flow reactor," Int. J Hyd. En., Vol. 29, no. 7, pp. 725–736, 2004.
[19] A. Kogan, M. Israeli, and E. Alcobi, "Production of hydrogen and carbon by solar thermal methane splitting. IV. Preliminary simulation of a confined tornado flow configuration by computational fluid dynamics," Int. J Hyd. En., vol. 32, no. 18, pp. 4800–4810, 2007.
[20] J. Yeheskel, and M. Epstein, "Thermolysis of methane in a solar reactor for mass-production of hydrogen and carbon nano-materials," Carbon, vol. 49, no. 14, pp. 4695–4703, 2011.
[21] N. Muradov, Z. Chen, and F. Smith, "Fossil hydrogen with reduced image emission: Modeling thermocatalytic decomposition of methane in a fluidized bed of carbon particles," Int. J Hyd. En., vol. 30, no. 10, pp. 1149–1158, 2005.
[22] D. Hirsch, M. Epstein, and A. Steinfeld, "The solar thermal decarbonization of natural gas," Int. J. Hydrogen Energy, vol. 26, pp. 1023–1033, 2001.
[23] J. K. Dahl, J. Tamburini, A. W. Weimer, A. Lewandowski, R. Pitts, and C. Bingham, "Solar-Thermal Processing of Methane to Produce Hydrogen and Syngas," Energy & Fuels, vol. 15, no. 5, pp. 1227–1232, 2001.
[24] S. Abanades and G. Flamant, "Production of hydrogen by thermal methane splitting in a nozzle-type laboratory-scale solar reactor," Int. J. Hydrogen Energy, vol. 30, no. 8, pp. 843–853, Jul. 2005.
[25] D. Trommer, "Kinetic investigation of the thermal decomposition of CH4 by direct irradiation of a vortex-flow laden with carbon particles," Int. J. Hydrogen Energy, vol. 29, no. 6, pp. 627–633, May 2004.
[26] J.K. Dahl, V.H. Barocas, D.E. Clough, and A.W. Weimer, "Intrinsic kinetics for rapid decomposition of methane in an aerosol flow reactor," vol. 27, pp. 377–386, 2002.
[27] S. Rodat, S. Abanades, and G. Flamant, "Co-production of hydrogen and carbon black from solar thermal methane splitting in a tubular reactor prototype," Sol. Energy, vol. 85, no. 4, pp. 645–652, 2011.
[28] A. Kacprzak, R. Kobyłecki, R. Włodarczyk, and Z. Bis, "The effect of fuel type on the performance of a direct carbon fuel cell with molten alkaline electrolyte," J. Power Sources, vol. 255, pp. 179–186, 2014.
[29] N. Muradov, P. Choi, F. Smith, and G. Bokerman, "Integration of direct carbon and hydrogen fuel cells for highly efficient power generation from hydrocarbon fuels," J. Power Sources, vol. 195, no. 4, pp. 1112–1121, 2010.
[30] S. Rodat, S. Abanades, J.L. Sans, and G. Flamant, "A pilot-scale solar reactor for the production of hydrogen and carbon black from methane splitting," Int. J. Hyd. En., vol. 35, no. 15, pp. 7748–7758, 2010.
[31] S. Rodat and G. Flamant, "High-Temperature Solar Methane Dissociation in a Multi-tubular Cavity-Type Reactor in the Temperature Range 1823 - 2073 K," vol. 44, no. 13, pp. 2666–2674, 2009.
[32] K. Hemmes, M. Houwing, and N. Woudstra, "Modeling of a Direct Carbon Fuel Cell System," J. Fuel Cell Sci. Technol., vol. 7, no. 5, pp. 051008, 2010.
[33] G. Cinti and K. Hemmes, "Integration of direct carbon fuel cells with concentrated solar power," Int. J. Hydrogen Energy, vol. 36, no. 16, pp. 10198–10208, 2011.
[34] The Linde Group, "Hydrogen Recovery by Pressure Swing Adsorption," Retrieved from http://www.linde-engineering.com.
[35] J. Larminie and A. Dicks, Fuel Cell Systems Explained. West Sussex, England: John Wiley & Sons, Ltd, 2003.
[36] N. Ozalp and B. Hyman, "Calibrated models of on-site power and steam production in the US manufacturing industries," Appl. Therm. Eng., vol. 26, no. 5–6, pp. 530–539, Apr. 2006.